JBC RESEARCH ARTICLE

ST3GAL1 regulates cancer cell migration through crosstalk between EGFR and neuropilin-1 signaling

Received for publication, February 6, 2025, and in revised form, February 20, 2025 Published, Papers in Press, February 28, 2025,
https://doi.org/10.1016/j.jbc.2025.108368

Tan-chi Fan[1], Hui Ling Yeo[1], Tsai-Hsien Hung[1], Nai-Chuan Chang[1], Yun-Hsin Tang[1,2,3], John Yu[1], Shih-Hsiang Chen[4,*], and Alice L. Yu[1,5,6,*]

From the [1]Institute of Stem Cell and Translational Cancer Research, Chang Gung Memorial Hospital, Linkou Branch, Taoyuan, Taiwan; [2]Department of Obstetrics and Gynecology, Chang Gung Memorial Hospital, Linkou Branch, and Chang Gung University, College of Medicine, Taoyuan, Taiwan; [3]Gynecologic Cancer Research Center, Chang Gung Memorial Hospital, Linkou Branch, Taoyuan, Taiwan; [4]Department of Pediatrics, Division of Hematology-Oncology, Chang Gung Memorial Hospital, Linkou Branch, and Chang Gung University, College of Medicine, Taoyuan, Taiwan; [5]Genomics Research Center, Academia Sinica, Taipei, Taiwan; [6]Department of Pediatrics/Hematology Oncology, University of California in San Diego, San Diego, California, USA.

Reviewed by members of the JBC Editorial Board. Edited by Robert Haltiwanger

Metastasis is a major cause of cancer-related morbidity and mortality. The overexpression of the sialyltransferase ST3GAL1 in breast cancer correlates with metastasis. However, the molecular mechanisms underlying the effect of ST3GAL1 on cell movement are poorly understood. We identified neuropilin-1/NRP1 as a substrate for ST3GAL1. Gene expression analysis revealed that recurrence-free survival (p = 0.0046) and distant metastasis-free survival (p = 0.0003) were significantly shorter in the ST3GAL1^{High}NRP1^{High} cohort than in the both-low subgroup. We demonstrated that the ST3GAL1-mediated sialylation of NRP1 results in increased binding affinity toward EGFR at the molecular level. At the cellular level, ST3GAL1 silencing impaired cell migration and wound healing ability, which was linked to reduced activities of CAPN2 as a consequence of diminished EGF/EGFR signaling. These data establish a function for the ST3GAL1-mediated sialylation of NRP1, leading to increased EGF/EGFR downstream signaling and enhanced tumor cell motility. Furthermore, ST3GAL1 silencing augmented the sensitivity to cetuximab-mediated cell lysis. Our findings provide novel insight into the mechanisms underlying the function of ST3GAL1 in promoting tumor cell migration through the EGFR/NRP1 pathway. Our results suggest that ST3GAL1 may represent a valuable target for strategies aimed at inhibiting tumor migration.

Altered glycosylation on the tumor cell surface can influence cell behaviors, such as cell adhesion, migration, and most importantly, the potential to invade or metastasize. For example, glycans on integrins may affect their structure and association with other surface receptors and thus downstream signaling. Abnormal sialylation promotes tumor invasion and metastasis in cancer cells (1). Sialidase-treated alpha5beta1 integrins exhibited enhanced binding to fibronectin, affecting cell adhesion and monocytic differentiation (2, 3). ST3 beta-galactoside alpha-2,3-sialyltransferase 1 (ST3GAL1) catalyzes the transfer of sialic acid in a α2,3 linkage to Gal-β1,3-GalNAc-Ser/Thr and thus terminates further chain elongation, except for extension with sialic acids (4). Altered expression levels or activity of this enzyme may lead to changes in the composition and length of *O*-glycans attached to mucin-type proteins. ST3GAL1 is highly expressed in breast, ovarian, colon, prostate, bladder, and hepatocellular carcinoma and glioblastoma (5). High expression of ST3GAL1 in breast cancer correlates with higher histologic grade and poor patient survival (6).

Neuropilin-1/NRP1 is a transmembrane protein that serves as an essential multifunctional cell surface coreceptor for many growth factors, including EGF, VEGF, FGF, and PDGF, to enhance downstream signaling (7). NRP1 is highly expressed in various cancers, especially advanced tumors, including breast, lung, and colorectal cancers, and is correlated with poor patient survival (8). NRP1 silencing severely suppresses mammosphere formation (9) and inhibits breast cancer cell migration and invasion (10). Blocking NRP1 function with an anti-NRP1 antibody prevents mammosphere formation (9) and suppresses gastric cancer xenograft tumor growth (11). Tumor metastasis is the leading cause of tumor-related mortality in cancer patients. Upregulated levels of NRP-1 in tumor tissues or circulating NRP1 are associated with nodal and distant metastasis in breast cancers (10, 12). Therefore, targeting the NRP1 pathway could effectively block breast cancer stem cell proliferation and tumor progression in breast cancer treatment.

Several studies have shown that 26 to 90% of breast cancers express EGFR (13–16), which is inversely correlated with ER status (16). Accumulating evidence has demonstrated that EGF/EGFR signaling may influence cancer progression through migratory pathways (17). EGFR is heavily *N*-glycosylated, and aberrant *N*-linked fucosylation has been shown to affect EGFR activity (18, 19). N-linked alpha2,6 sialylation promotes EGFR signaling by facilitating receptor oligomerization and recycling (20). However, *O*-linked glycosylation sites on EGFR have not been reported (21). It has been shown

* For correspondence: Alice L. Yu, a1yu@health.ucsd.edu; Shih-Hsiang Chen, samechen@cgmh.org.tw.

that NRP1 interacts with EGFR, regulates EGF-induced EGFR clustering on the cell surface and elicits downstream signaling in lung cancer and prostate cancer cells (22, 23). NRP1 is a transmembrane protein composed of a large N-terminal extracellular region and a small cytoplasmic tail (24). The extracellular domain of NRP1 contains three *N*-glycosylation sites and is heavily *O*-glycosylated (25). Since the extracellular domain of NRP1 interacts with EGFR and promotes downstream AKT signaling activation (23), we investigated whether *O*-linked sialylation of NRP1 affects EGFR signaling and cell motility in breast cancer cells.

In this study, we demonstrated that upon ST3GAL1 silencing in breast cancer cells, the expression of total NRP1 and EGFR proteins was not affected, but the cells displayed decreased migration and invasion ability. We showed that the ST3GAL1-mediated sialylation of NRP1 resulted in increased binding affinity for EGFR. The impaired cell migration, invasion, and wound healing ability upon ST3GAL1 silencing was linked to reduced activities of calpain 2 because of attenuated EGF/EGFR signaling. To our knowledge, this is the first study to show that the *O*-sialylation of NRP1 plays an important role in binding to EGFR and regulating cell migration. Most importantly, breast cancer patients with high ST3GAL1 expression had significantly worse distant metastasis-free survival than those with low ST3GAL1 expression.

Results

NRP1 is a protein target of ST3GAL1

Nonsialylated Galβ1-3GalNAc-Ser/Thr, a core 1 *O*-glycan, is a ligand for PNA lectin (26). When this *O*-disaccharide is modified by the addition of sialic acid to the α2-3 linkage, it generates trisaccharide sialyl 3T, which is no longer recognized by the PNA lectin. Previously, we observed enhanced plant lectin peanut agglutinin (PNA) binding in *ST3GAL1*-silenced breast cancer cells (6) and identified several ST3GAL1-targeted proteins using a PNA lectin pull-down assay in breast cancer cells (6, 27, 28). We found NRP1 to be an *O*-linked sialoprotein. Western blot analysis revealed that the total amount of NRP1 was unchanged after *ST3GAL1* silencing, but NRP1 immunoprecipitated from *ST3GAL1* silenced MDA-MB-231 cells exhibited more PNA-positive signals (Fig. 1*A*), which likely reflected the greater number of core 2-base structures after *ST3GAL1* silencing. The efficiency of *ST3GAL1* silencing was assayed by qPCR analysis as shown in Figure S1*A*. We also assessed the surface expression of EGFR and NRP1 using flow cytometry. No significant differences were observed following *ST3GAL1* silencing, consistent with the Western blot analysis findings (Fig. 1*C*).

ST3GAL1 regulates EGF-mediated EGFR/NRP1 signaling

To investigate the role of posttranslational modifications of NRP1 in EGFR signaling in breast cancer cells, we used the MDA-MB-231 cell line, which expresses both NRP1 and EGFR, as shown by Western blot analysis (Fig. S1*B*). NRP1 depletion in MDA-MB-231 cells by shRNA transfection (Fig. 2*A*) significantly decreased EGF-induced EGFR phosphorylation without affecting the total amount of EGFR protein (Fig. 2*A*). Because the extracellular domain of NRP1 interacts with EGFR (22, 23), we wondered whether the ST3GAL1-mediated sialylation of NRP1 affects EGFR

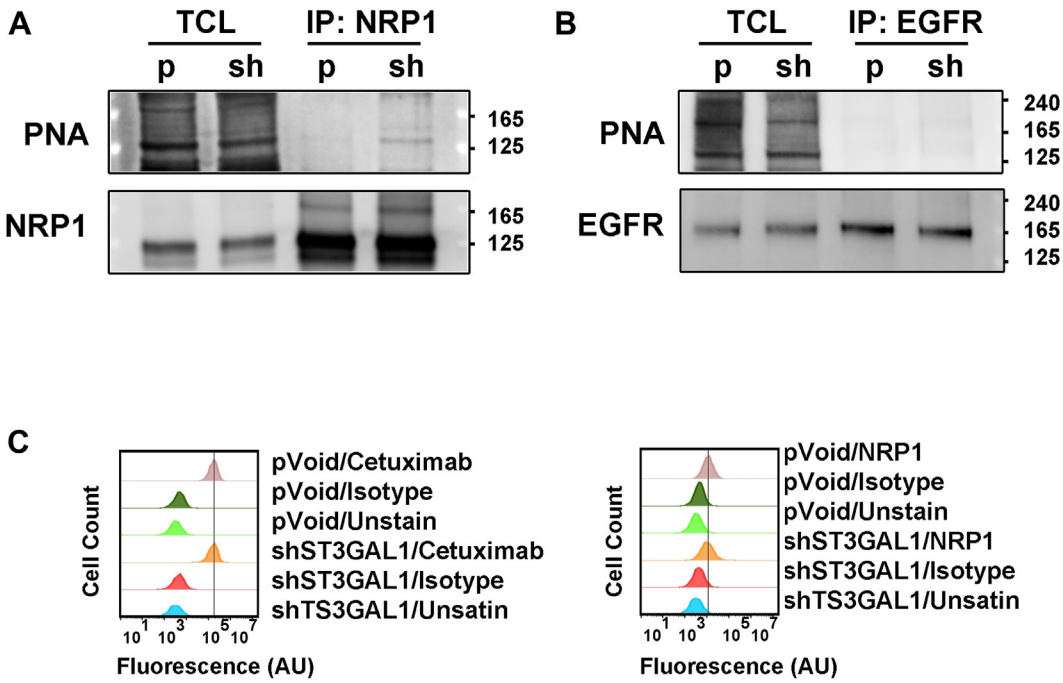

Figure 1. Identification of NRP1 as an ST3GAL1 target protein. Cell extracts from MDA-MB-231 cells transfected with control pVoid or *shST3GAL1* were immunoprecipitated with (*A*) NRP1 antibody or (*B*) EGFR antibody, followed by immunoblotting with biotinylated PNA lectin, NRP1 or EGFR antibody. There was a greater PNA binding signal in purified NRP1 from *shST3GAL1* transfected MDA-MB-231 cells. There was no PNA signal on the purified EGFR. *C*, the EGFR and NRP1 on the cell surface were assessed by staining cells with cetuximab and anti NRP1 antibody, followed by goat anti-human IgG-AF488 or goat anti-rabbit IgG-AF488 staining, respectively. p, control pVoid shRNA; sh, *ST3GAL1* shRNA.

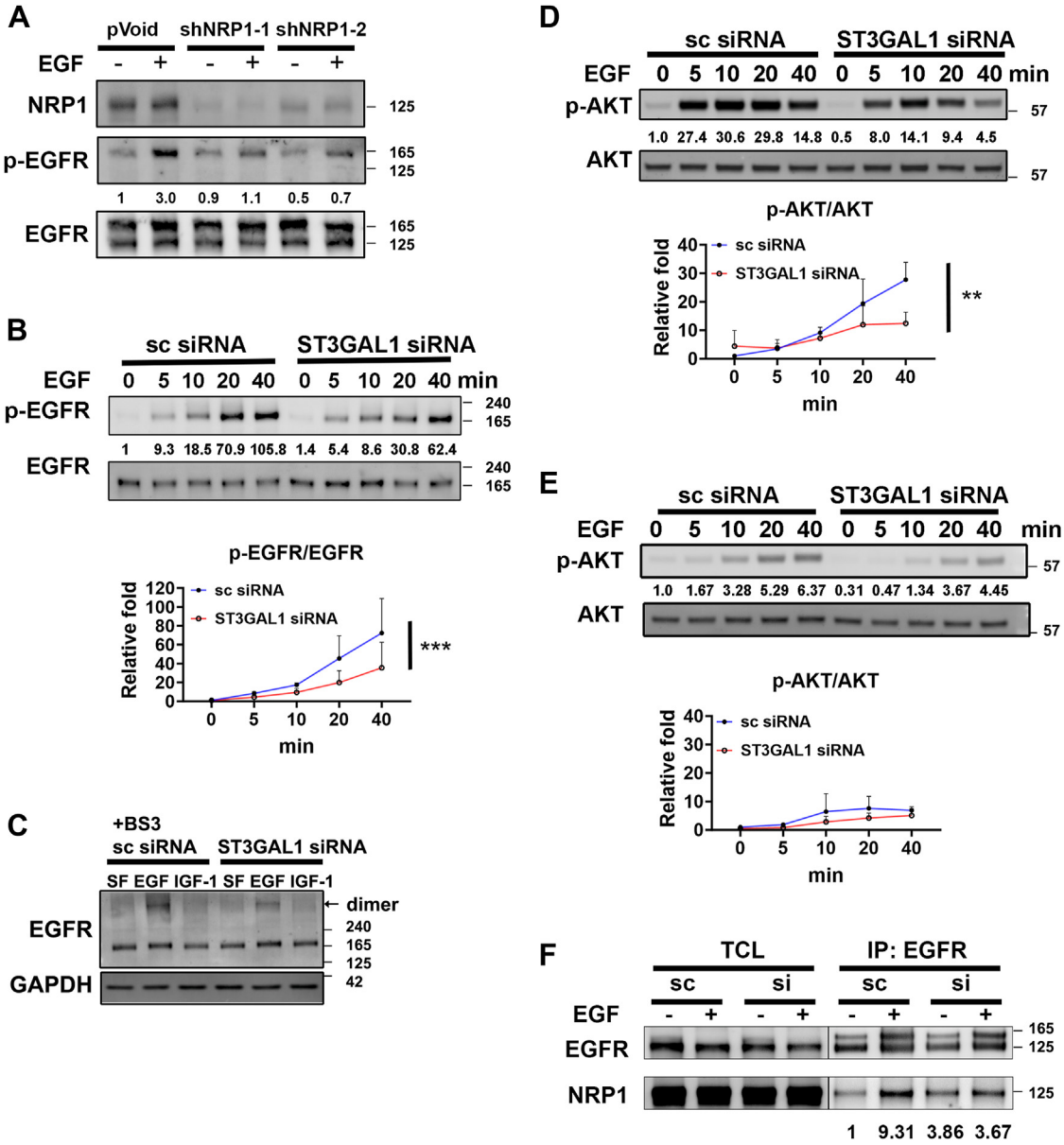

Figure 2. Silencing of *ST3GAL1* diminished EGF-induced downstream signaling. *A*, control pVoid- or *NRP1* shRNA transfected MDA-MB-231 cells were incubated in serum-free media overnight and then treated with 15 ng/ml EGF for 10 min. Cell extracts were subjected to NuPAGE and Western blotting with the indicated antibodies. MDA-MB-231 cells (*B, D*) and SKBR3 cells (*E*) were transfected with control (sc) or *ST3GAL1* siRNA, followed by incubation with 15 ng/ml EGF. Cell extracts obtained at the indicated times were subjected to Western blotting with the indicated antibodies. The intensity of each phosphoprotein band was normalized to that of the total protein band. The mean ± S.D. relative fold of densitometric analyses is shown from n = 3 independent experiments. *C*, control or *ST3GAL1* siRNA transfected MDA-MB-231 cells were incubated in serum-free media overnight and then treated with 15 ng/ml EGF or IGF-1 for 10 min, followed by crosslinking using BS^3. Cell extracts were subjected to nonreducing NuPAGE and Western blotting with the indicated antibodies. *F*, control or *ST3GAL1* siRNA transfected MDA-MB-231 cells were serum-starved overnight, followed by incubation with 10 ng/ml EGF for 15 min. EGFR was immunoprecipitated from cell lysates as shown by western blotting analysis. The intensity of coimmunoprecipitated NRP1 was first normalized to that of immunoprecipitated EGFR and then normalized to the ratio of coimmunoprecipitated NRP1/EGFR in control cells without EGF treatment. Representative images are shown. sc, control scramble siRNA; si, *ST3GAL1* siRNA; SF, serum-free; BS^3, bis(sulfosuccinimidyl) suberate. $^{**}p < 0.01$, and $^{***}p < 0.001$ by two-tailed Student's *t* test.

signaling in breast cancer cells. Although *ST3GAL1* silencing in MDA-MB-231 cells increased the PNA signal on NRP1, there was no PNA signal on EGFR, indicating that EGFR was not a protein target of ST3GAL1 (Fig. 1*B*).

We found that EGF-induced EGFR phosphorylation was significantly decreased when *ST3GAL1* was silenced by siRNA (Fig. 2*B*). EGF-stimulated EGFR dimerization was also decreased by *ST3GAL1* silencing (Fig. 2*C*). Consistent with these findings, our Western blot results showed that *ST3GAL1* silencing impeded EGF-induced AKT phosphorylation in MDA-MB-231 cells (Fig. 2*D*), but this effect was less significant in $NRP1^{Low}$ SKBR3 cells (Fig. 2*E*). Furthermore, a coimmunoprecipitation assay demonstrated that NRP1 was basally associated with EGFR in breast cancer cells and that EGF strongly enhanced the formation of this complex, which was not observed in *ST3GAL1* silenced cells (Fig. 2*F*). Since there

are no *O*-linked glycosylation sites on EGFR, these findings strongly suggest that *O*-linked sialylation of NRP1 may promote EGF-induced EGFR phosphorylation and clustering, with subsequent downstream signaling in breast cancer cells. A similar phenomenon was observed in A549 and ASB145-1R cells, in which both EGF-induced EGFR phosphorylation, AKT phosphorylation and the EGFR/NRP1 interaction were decreased when *ST3GAL1* was silenced (Figs. S2 and S3, respectively).

ST3GAL1-mediated O-linked sialylation of NRP1 is important for its interaction with EGFR

To determine the binding affinities of NRP1 for the EGF/EGFR complex at the molecular level *in vitro*, the HA-tagged extracellular domain of NRP1 (HA-NRP1) was expressed in MDA-MB-231 control pVoid or *shST3GAL1* stable clones (Fig. 3*A*). HA-NRP1 was purified by capture onto anti-HA antibody-conjugated sepharose beads, followed by release with HA peptide and extensive dialysis with PBS. The purified

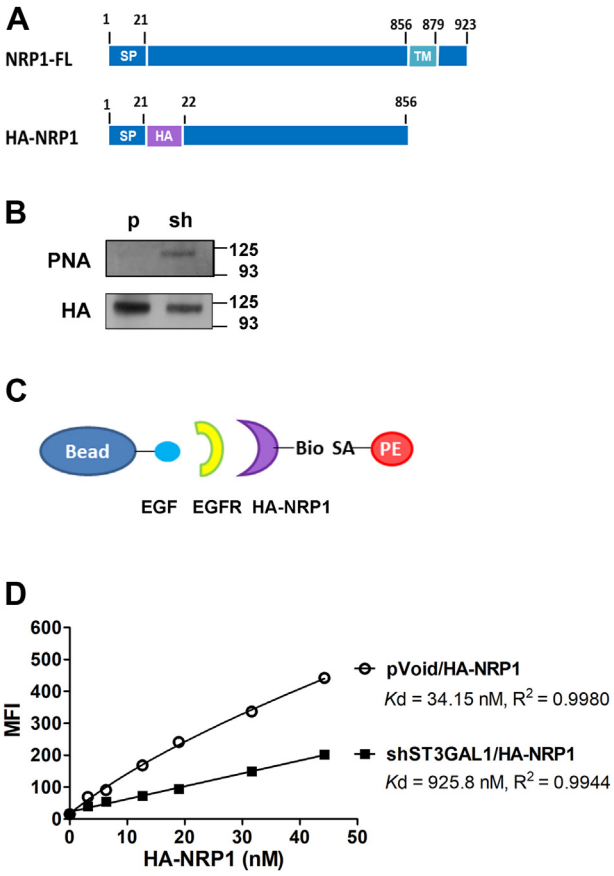

Figure 3. *O*-linked sialylation of HA-NRP1 promoted HA-NRP1/EGF/EGFR complex formation. *A*, schematic diagram of HA-NRP1 plasmid construction. *B*, culture media of MDA-MB-231 cells transfected with purified HA-NRP1 from control pVoid or *shST3GAL1* were immunoblotted with biotinylated PNA lectin and HA antibody. *C*, schematic diagram of the Luminex immunosandwich assay. *D*, binding saturation curves of Luminex fluorescence intensities between the EGF/EGFR complex and purified HA-NRP1 from control pVoid- or *shST3GAL1* transfected MDA-MB-231 cells were generated. The *Kd* values were determined by nonlinear regression analysis using GraphPad Prism 5.01. p, control pVoid shRNA; sh, *ST3GAL1* shRNA; SP, signal peptide; HA, HA tag; TM, transmembrane region.

shST3GAL1/HA-NRP1 exhibited more PNA-positive signals than did the control pVoid/HA-NRP1, as determined by Western blot analysis (Fig. 3*B*). This result is consistent with the effect of *ST3GAL1* silencing on endogenous NRP1 in MDA-MB-231 cells (Fig. 1). To demonstrate that the sialylation of NRP1 could increase the binding affinity between NRP1 and the EGF/EGFR complex (Fig. 3*C*), recombinant EGF was coupled to MagPlex beads and then incubated with EGFR overnight, followed by incubation with increasing concentrations of biotinylated HA-NRP1. The bound biotinylated HA-NRP1 was then quantified using streptavidin-conjugated phycoerythrin, as determined by the Luminex 200 instrument. EGF-coupled beads without incubation with biotinylated HA-NRP1 were used as negative controls. The binding saturation curves and dissociation constants (*K*d) were determined by nonlinear regression analysis with GraphPad Prism 5.01 (Fig. 3*D*), and the *K*d values of the control HA-NRP1 and *shST3GAL1*/HA-NRP1 were 34.15 nM and 925.8 nM, respectively. The R^2 value was 0.99 for both the control and desialylated NRP1 strains. The results showed that *O*-linked sialylated biotinylated HA-NRP1 displayed greater binding affinity for the EGF/EGFR complex than did desialylated biotinylated HA-NRP1 (Fig. 3*D*). These data were consistent with the coimmunoprecipitation results at the cellular level (Fig. 2*F*), showing that *O*-linked sialylation of NRP1 increased its binding affinity for the EGF/EGFR complex.

LC–MS/MS analysis revealed alpha2,3 sialylation to be the dominant O-glycan structure of NRP1

To delineate *O*-glycans on NRP1, the protein band on NuPAGE corresponding to purified endogenous NRP1 was excised and subjected to in-gel tryptic digestion. Total glycopeptides were isolated and analyzed using liquid chromatography-tandem mass spectrometry (LC–MS/MS). Figure 4*A* shows a schematic representation of the NRP1 protein domains and site-specific *O*-glycosylation sites with high confidence. All the identified *O*-glycosylation sites from NRP1, including the retention times determined by LC–MS/MS, mass–charge ratios (m/z) of *O*-glycan ions, structural information, and relative abundance, are summarized in the Materials and Methods section. The upper part of Figure 4*A* displays *O*-glycans identified from NRP1 purified from control MDA-MB-231 cells, while the lower part shows *O*-glycans of NRP1 from *ST3GAL1* silenced MDA-MB-231 cells. Notably, T827, T830, and S844 in the control MDA-MB-231 cells carried sialyl 3T, the cancer-relevant *O*-glycan catalyzed by ST3GAL1. In contrast, branched *O*-glycans were detected after ST3GAL1 downregulation. Figure 4, *B* and *C* show the HCD MS/MS spectra of the doubly charged glycopeptides corresponding to glycopeptide T830 derived from control or *ST3GAL1* knockdown cells, respectively. These data indicated that the major glycoforms corresponding to sialyl 3T were converted to branched *O*-glycans after *ST3GAL1* silencing. The glycoforms identified from T827, T830, and S844 are shown in Figure S4.

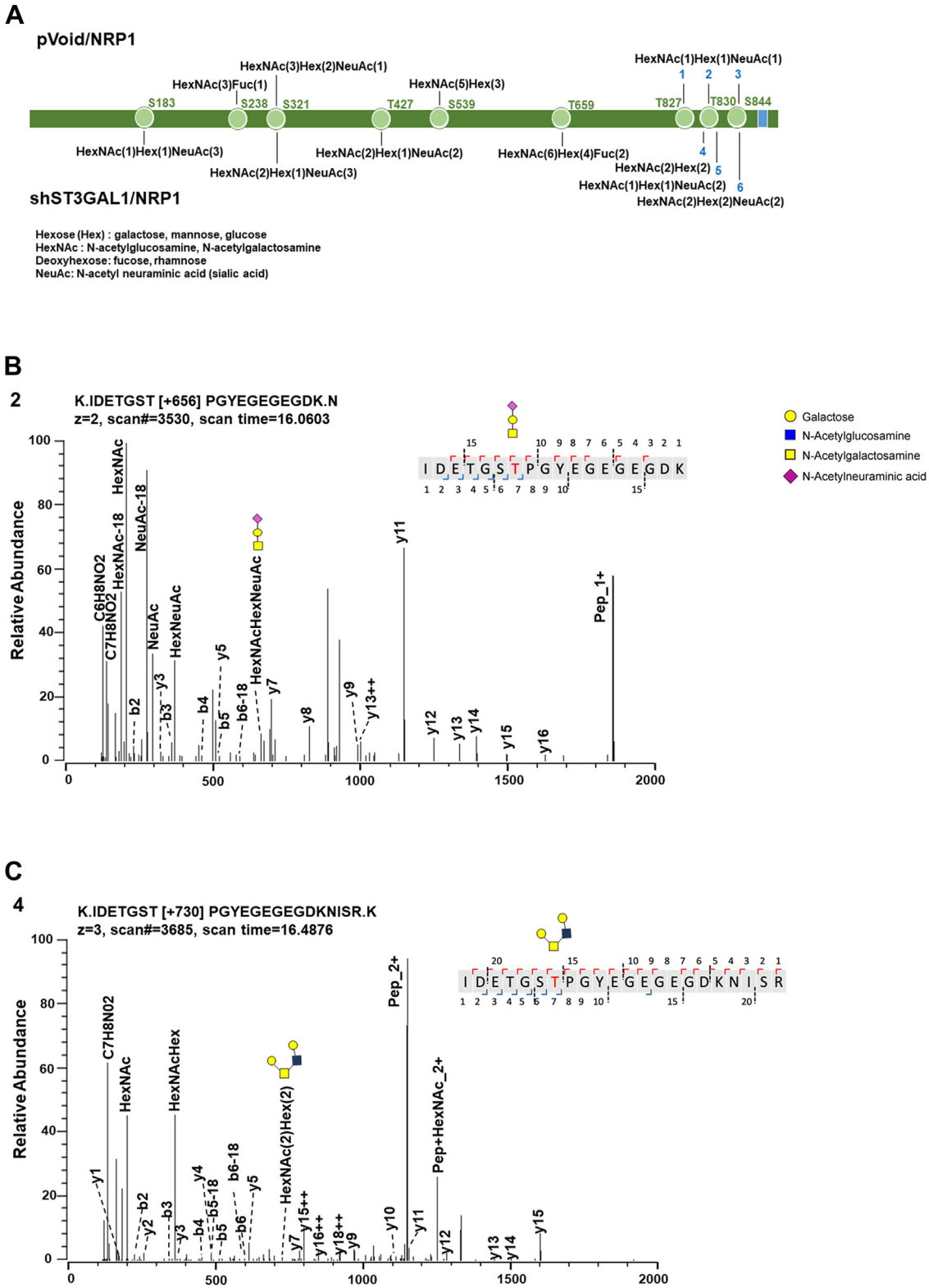

Figure 4. *O*-linked glycan profiles of endogenous NRP1 purified from MDA-MB-231 cells. *A*, schematic representation of site-specific annotation of the *O*-glycan structure of endogenous NRP1 purified from MDA-MB-231 cells transfected with control pVoid or *shST3GAL1*. The positions of individual *O*-glycosylation sites are indicated by their amino acid number along the primary sequence of NRP-1. The blue segment represents the transmembrane domain. Upper *O*-glycans were identified in the control pVoid/NRP1, while lower *O*-glycans were identified in the *shST3GAL1*/NRP1. Glycan structures that were confirmed by glycopeptide analysis with high confidence are shown schematically with the individual symbols defined. Major glycoforms identified on T830 from control pVoid/NRP1 (*B*) or *shST3GAL1*/NRP1 (*C*) are shown along with the HCD MS/MS spectra of the doubly charged glycopeptides, corresponding to the most abundant glycoforms. The accurately measured m/z values of peptide b and y ions with and without a single HexNAc at Thr/Ser, together with the peptide backbone and peptide backbone + HexNAc, are shown.

ST3GAL1 regulates NRP1 signaling

ST3GAL1 regulated EGF-induced CAPN2 phosphorylation

Overexpression of ST3GAL1 in cancer cells increased cell migration and invasion (29, 30). To further validate the role of ST3GAL1 in cell movement, *ST3GAL1* was silenced in the MDA-MB-231 breast cancer cell line, and cell migration was subsequently monitored using an *in vitro* scratch assay. As shown in Fig. 5*A*, the motility of *ST3GAL1*-silenced cells was significantly slower than that of the control cells. Transwell migration of *shST3GAL1*-transfected MDA-MB-231 cells was also significantly reduced to approximately 30% of the control (Fig. 5*B*). A similar trend was observed in *shNRP1*-transfected MDA-MB-231 cells (Fig. S5*A*). Furthermore, EGF-induced Transwell migration of *shST3GAL1* cells decreased to approximately 20% of the control (Fig. 5*B*). More strikingly, the Transwell invasion of *shST3GAL1* cells was reduced to 10% of the control (Fig. 5*B*). A comparable effect was observed in *shST3GAL1*-transfected ASB145-1R cells (Fig. S6*A*). These data clearly demonstrated that *NRP1* or *ST3GAL1* silencing impacts cell migration.

Calpain activity plays a crucial role in fibroblast invadopodia formation and tail retraction during migration (31). EGF/EGFR-induced cell motility is mediated through the phosphorylation and activation of calpain-2 (CAPN2), which regulates focal adhesion turnover to facilitate efficient cell migration. The disassembly of focal adhesions was assessed by the ratio of CAPN2-cleaved Talin to its full-length form (32). In *shST3GAL1*-transfected MDA-MB-231 cells, the ratio of cleaved Talin was significantly reduced (Fig. 5*C*). To confirm the reduction in calpain activity following *ST3GAL1* silencing, casein zymography was performed. As shown in Figure 5*D*, control MDA-MB-231 cells exhibited strong CAPN1 and CAPN2 activities. In contrast, *ST3GAL1*-silenced cells displayed a significant reduction in CAPN2 activity, while CAPN1 activity remained unaffected.

To further investigate the molecular mechanisms underlying ST3GAL1-mediated cell motility, we examined the effects of *ST3GAL1* and *NRP1* silencing on phosphorylated CAPN2, a key indicator of CAPN2 activity, in response to EGF stimulation. EGF-induced phospho-CAPN2 level was significantly higher in control cells compared to *shST3GAL1*-or *shNRP1*-transfected cells, as shown in Figures 5*C* and S5*B*, respectively. CAPN2 activity was further demonstrated by Talin cleavage, as determined by Western blot analysis. The ratio of EGF-induced cleaved Talin was significantly higher in control cells compared to *shST3GAL1*-or *shNRP1*-transfected cells (Fig. 5*C* and S5*B*).

A similar effect was observed in *shST3GAL1*-transfected ASB145-1R cells (Fig. S6, *B–D*), where *ST3GAL1* silencing reduced EGF-induced calpain phosphorylation and Talin cleavage. However, EGF failed to induce CAPN2 phosphorylation or Talin cleavage in $EGFR^{Low}$ MCF7 cells (Fig. 5*F*). In addition, qPCR analysis confirmed that EGF stimulation had no significant effect on CAPN1 or CAPN2 transcription (Fig. 5*G*). Taken together, these findings strongly suggest that cell surface α2,3-sialylation contributes to NRP1/EGFR-mediated breast cancer cell detachment and motility.

Correlation analysis of gene expression and survival

Finally, we assessed the clinical relevance of ST3GAL1 and NRP1 expressions using the publicly available dataset GSE47561, which contains expression data from 1570 breast cancer samples. As shown in Fig. 6, the expression levels of ST3GAL1 (median expression value: 4.44 *versus* 4.36, $p < 0.0001$) and NRP1 (median expression value: 7.68 *versus* 7.61, $p = 0.04$) were significantly greater in breast cancer patients with metastasis than in those without metastasis (Fig. 6, *A* and *B*). To further evaluate the combined effect of ST3GAL1 and NRP1 expression, patients were stratified into four groups for Kaplan–Meier survival analysis: $ST3GAL1^{Low}NRP1^{Low}$, $ST3GAL1^{Low}NRP1^{High}$, $ST3GAL1^{Low}NRP1^{High}$, and $ST3GAL1^{High}NRP1^{High}$. Relapse-free survival (RFS) was not different between the $ST3GAL1^{Low}NRP1^{Low}$ cohort and the $ST3GAL1^{Low}NRP1^{High}$ ($p = 0.81$) or $ST3GAL1^{Low}NRP1^{High}$ ($p = 0.55$) cohorts. A comparison of the patients in the $ST3GAL1^{Low}NRP1^{Low}$ and $ST3GAL1^{High}NRP1^{High}$ cohorts revealed that the latter had significantly worse RFS than did the both-low group ($p = 0.0046$) at 1 year (97% *versus* 93.9%), 5 years (67.8% *versus* 77.2%), and 10 years (48.4 *versus* 68.7%) (Fig. 6*C*). More importantly, patients with both high ST3GAL1 and high NRP1 expression had significantly worse distant metastasis-free survival (DMFS) than patients in the both-low group ($p = 0.0003$) at 1 year (93.7% *versus* 98.1%), 5 years (71.5% *versus* 79.9%), and 10 years (55.2% *versus* 78.7%) (Fig. 6*D*). These data indicate that the low expression of ST3GAL1 and NRP1 is correlated with favorable distant metastasis-free survival.

ST3GAL1 silencing enhances cetuximab-induced antibody-dependent cellular cytotoxicity (ADCC) and inhibits cell growth

Cetuximab, an anti-EGFR chimeric IgG1 monoclonal Ab, binds to the extracellular domain of EGFR and induces receptor internalization, thereby preventing downstream signaling (33). Additionally, cetuximab can induce cell death *via* NK cell-mediated ADCC. NK cells express the inhibitory receptor Siglec-7, which, when bound to its ligand on target cells, prevents the lysis of target cells (34). It has been shown that *ST3GAL1* silencing reduces the expression of Siglec-7 ligands on tumor cells (35). We investigated whether cetuximab-mediated ADCC activity was dampened by ST3GAL1-mediated sialylation on the surface of cancer cells in the presence of 0.25 μg/ml cetuximab. Peripheral blood mononuclear cells (PBMCs) induced 14.8% lysis of control pVoid cells, which was significantly less than the 28.4% ADCC activity against *shST3GAL1* cells (Figs. 7*A*, and S7*A*). Thus, ST3GAL1 expression protects cancer cells from PBMC-mediated cytolysis.

Cetuximab alone cannot effectively inhibit the proliferation of MDA-MB-231 cells (31, 36). To further investigate whether targeting *O*-linked sialylation could enhance cancer cell sensitivity to cetuximab *in vitro*, continuous cell growth was monitored using the xCELLigence system. *ST3GAL1* silencing

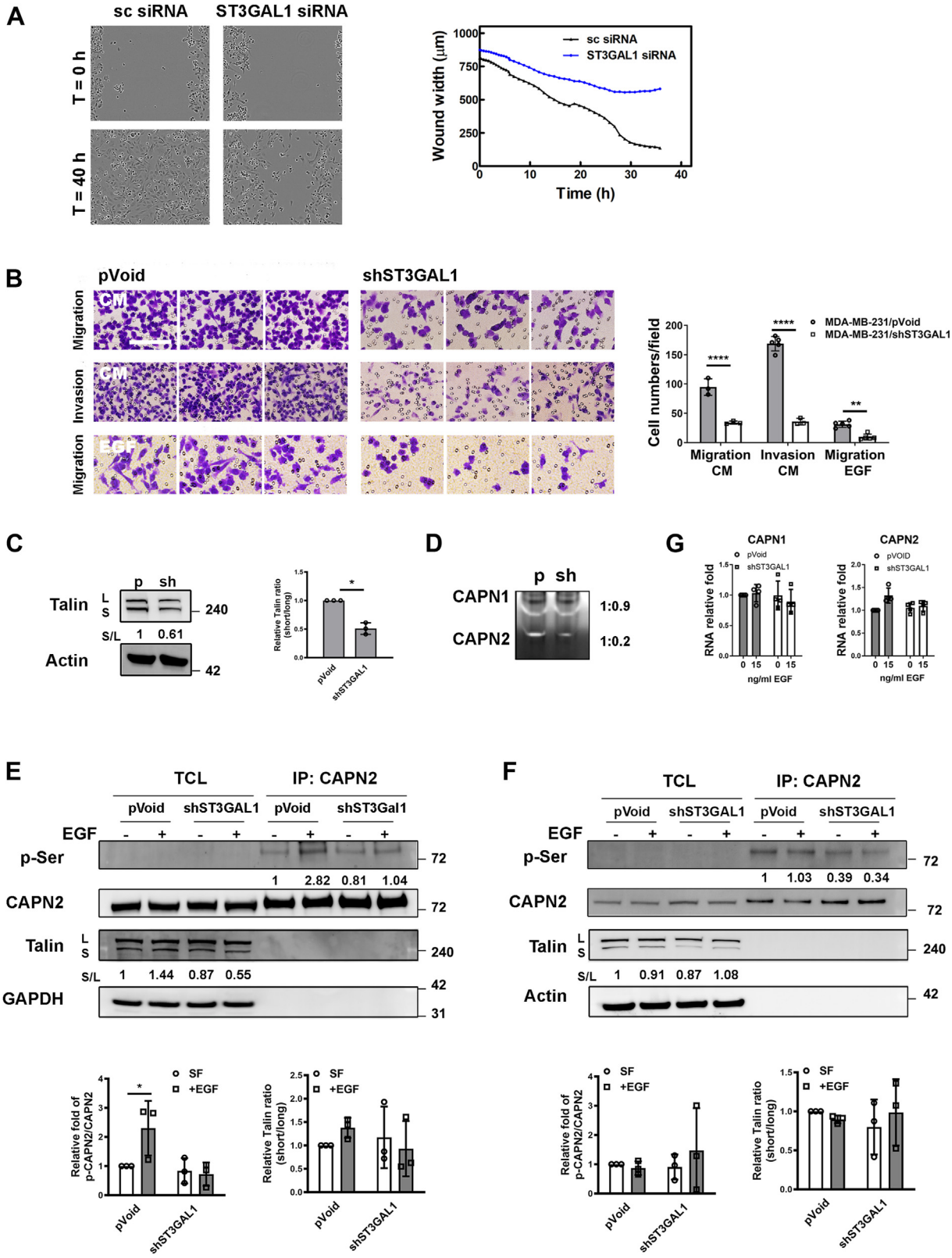

Figure 5. ST3GAL1 regulates cell migration. *A*, the wound healing ability of MDA-MB-231 cells transfected with control sc or *ST3GAL1* siRNA was assessed. *B*, migration and invasion assays were performed using Transwell inserts, either untreated for the migration assay or coated with Matrigel for the invasion assay. MDA-MB-231 cells transfected with control pVoid or *shST3GAL1* were added to the *upper* chamber of Transwell inserts. The *lower* chamber was filled with complete culture medium (CM) or 100 ng/ml EGF in serum free media for transwell migration assay. Cells that invaded the inverse side of the membrane were stained with crystal *violet* and counted. Data are presented as the mean cell numbers/field ± standard deviation, based on representative results from three independent experiments (n = 3). Statistical significance was determined using the two-way ANOVA with multiple comparisons. Scale bar = 100 um. *C*, total cell lysates from control pVoid- or *shST3GAL1*-transfected MDA-MB-231 cells were processed for Western blotting with a talin antibody. The intensity of the cleaved form (short) was first normalized to that of the full-length form (long) and then normalized to the short/long ratio of

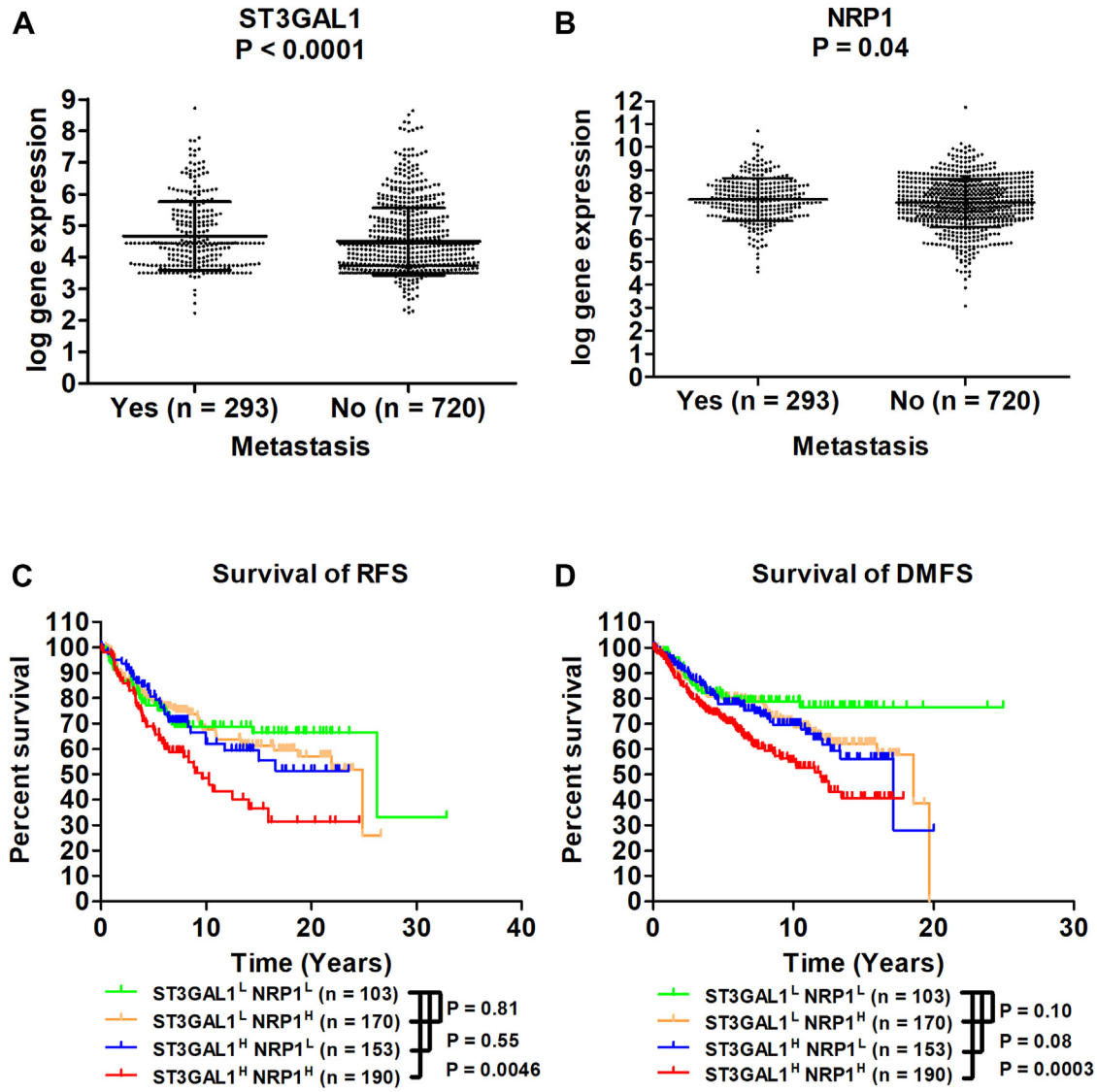

Figure 6. Analysis of survival outcomes in patients with different expression levels of ST3GAL1 and NRP1 using the breast cancer dataset GSE47561. ST3GAL1 (*A*) and NRP1 (*B*) expression levels are shown as boxplots of log gene expression values in breast cancer patients with and without metastasis in the GSE47561 dataset. A two-tailed Student's *t* test was applied for statistical comparison. Kaplan-Meier curves showing the relapse-free survival (RFS) (*C*) and distant metastasis-free survival (DMFS) (*D*) of patients with breast cancer according to combined ST3GAL1 and NRP1 expression. The log-rank test was applied for statistical comparison. H, high; L, low.

clearly reduced cell growth compared to that in control cells (Fig. 7*B*, and S7*B*). High concentrations of cetuximab can also inhibit cell growth. Cetuximab treatment further decreased the proliferation of *ST3GAL1* silenced cells (Fig. 7*B*). Therefore, *O*-linked sialylation may enhance the efficacy of cetuximab in patients with breast cancer, both directly and indirectly, through NK-mediated ADCC.

Discussion

EGFR overexpression in breast cancer is associated with a more aggressive phenotype and is prone to lymph node metastasis (32). Aberrant glycosylation or sialylation can affect EGFR activity (18, 19). Here, we demonstrated that EGFR signaling can be modulated by the sialylation status of the EGFR coreceptor NRP1. The activation of EGFR downstream

the control cells. Data are presented as the mean relative ratio ± standard deviation, based on representative results from three independent experiments (n = 3). Statistical significance was determined by two-tailed Student's *t* test. *D*, zymography showing changes in calpain activity after *ST3GAL1* silencing in MDA-MB-231 cells. MDA-MB-231 (*E*) or MCF7 (*F*) cells transfected with control pVoid or *shST3GAL1* were serum starved overnight and then treated with 10 ng/ml EGF for 30 min. CAPN2 was immunoprecipitated from cell lysates and processed for Western blotting with phospho-serine and CAPN2 antibodies. The intensity of phospho-serine was first normalized to that of immunoprecipitated CAPN2 and then normalized to the ratio of phospho-serine/CAPN2 in control cells without EGF treatment. Representative images are shown. Data are presented as the mean relative fold of p-CAPN2/CAPN2 or Talin ratio ± standard deviation, based on representative results from three independent experiments (n = 3). Statistical significance was determined using the two-way ANOVA with multiple comparisons. *G*, control or *ST3GAL1*-silenced MDA-MB-231 cells were treated with 15 ng/ml EGF for 2 h. The transcription of the indicated genes was measured and normalized to that of GAPDH by qPCR analysis. Data are presented as the mean relative fold ± standard deviation, based on representative results from three independent experiments (n = 3). p, control pVoid shRNA; sh, *ST3GAL1* shRNA; SF, serum free. $*p < 0.05$, $**p < 0.01$, $***p < 0.001$, $****p < 0.0001$.

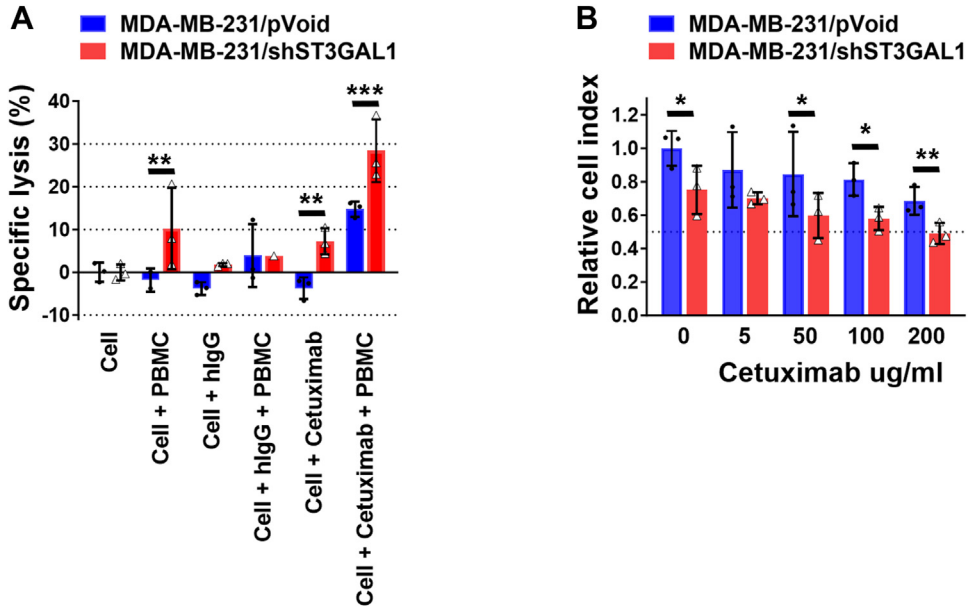

Figure 7. The combination of *ST3GAL1* silencing and cetuximab significantly enhanced the sensitivity of cells to PBMC-induced cell lysis. *A*, PBMC-mediated lysis activity against MDA-MB-231 control pVoid or *shST3GAL1* stable clones was evaluated at an E:T ratio of 20:1. Tumor lysis was assessed by measuring BATDA after 3.5 h of incubation of human PBMCs with MDA-MB-231 control pVoid or *shST3GAL1* stable clones with or without the indicated antibodies. Nonspecific human IgG was used as a negative control. One representative donor of 3 total donors is shown. *B*, cControl or *shST3GAL1* transfected MDA-MB-231 cells cultured in complete media supplemented with or without cetuximab were monitored for 72 h using the xCELLigence System. The images shown are representative of three experiments. $*p < 0.05$, $**p < 0.01$, and $***p < 0.001$ by two-tailed Student's *t* test.

signaling induces the activation of calpain 2, thereby regulating cell migration and metastasis (14, 37). Here, we demonstrated that reduced sialylation of NRP1 diminished its interaction with the EGFR/EGF complex, thereby decreasing the activation of EGFR downstream signaling, as illustrated in Fig. 8. This phenomenon was not observed in the NRP1-negative cell line. Moreover, the EGF-induced phosphorylation of CAPN2 was downregulated when *ST3GAL1* was silenced. As CAPN2-mediated proteolysis of focal adhesion complexes could release

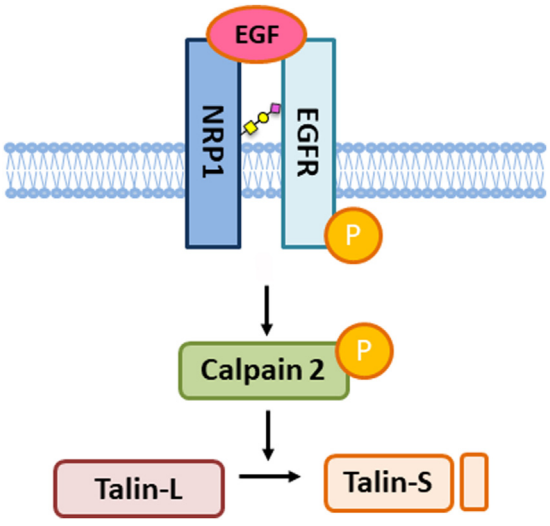

Figure 8. Proposed schema illustrating the role of ST3GAL1 in modulating the signaling network of NRP1/EGFR in breast cancer cells. *O*-linked sialylation of NRP1 increased cell migration by facilitating NRP1/EGFR interaction and downstream signaling.

cell-substratum adhesiveness and allow for efficient cell migration, it is not surprising that high expression of ST3GAL1 and NRP1 was correlated with worse distant metastasis-free survival. This finding is consistent with a report that NRP1 expression was significantly greater in patients with breast cancer having lymph node involvement than in those without lymph node involvement (38). Moreover, high serum levels of soluble NRP1 are an independent marker of poor prognosis in patients with early-stage breast cancer (39). NRP1 depletion leads to the downregulation of MMP2 and MMP9 (40). Therefore, NRP1 may be an indicator of metastatic potential in breast cancer, as demonstrated in this study.

The high molecular weight form of NRP1 is modified by the addition of chondroitin sulfate (CS) to a serine residue (Ser612) (41). Overexpression of the NRP1 S612A mutation in U87MG glioma cells leads to the loss of CS modification and thus enhanced cell invasiveness. The major form of NRP1 in breast cancer cell lines is a low molecular weight protein with little CS modification (Fig. S1*B*). Here, we demonstrated that *O*-linked sialylation of NRP1 is associated with increased invasion of cancer cells. Our glycopeptide analysis identified several *O*-linked glycosylation sites that have not been previously reported (S183, S238, S321, T427, S539, and T659). Most importantly, the regions (T827, T830, and S844) near the transmembrane region (T857-T879) of NRP1 were decorated with sialyl 3T glycans, which were not detected when *ST3GAL1* was silenced. The effect of sialyl 3T glycans in this region on protein–protein interactions warrants further investigation.

Several EGFR inhibitors that block EGFR signaling have been evaluated in metastatic breast cancer. Cetuximab alone

cannot effectively inhibit the proliferation of MDA-MB-231 cells (31, 36). The EGFR kinase inhibitor gefitinib (Iressa) has been used in combination with trastuzumab (Herceptin) to treat HER2-positive metastatic breast cancer (42). However, this combination therapy did not improve overall survival compared to trastuzumab alone, despite most of the cancer tissues exhibiting EGFR overexpression. The molecular mechanism underlying the insensitivity to EGFR-targeted therapy in patients with metastatic breast cancer is unclear. However, cetuximab alone cannot effectively inhibit MDA-MB-231 cell viability (36). Here, we demonstrated that silencing *ST3GAL1* in MDA-MB-231 cells can enhance their sensitivity to cetuximab by decreasing EGFR dimerization and phosphorylation. Taken together, these findings indicate that *ST3GAL1* silencing modulates the NRP1/EGFR interaction, EGFR dimerization on the cell surface, and thus downstream signaling, suggesting that there is functional crosstalk between the ST3GAL1, NRP1, and EGFR pathways in cancer cells.

In summary, we demonstrated that *ST3GAL1* silencing affects breast cancer cell motility by inhibiting the NRP1/EGFR pathway. The glycan profiles of NRP1 showed that *ST3GAL1* silencing reduced the expression of sialyl 3T, impeding the migration and invasion of breast cancer cells. We also showed that the activities of CAPN2 was decreased in *ST3GAL1* silenced cells. These data suggest that *O*-glycans and sialyl 3T modification by ST3GAL1 promote the invasiveness of breast cancer cells.

Experimental procedures

Cells, antibodies, and reagents

The ASB634, ASB145-1R, and ASB244-1R breast cancer cell lines were established in our laboratory (43). ZR-75-1 was kindly provided by Dr Jin-Yuh Shew (Academia Sinica). All other cancer cell lines were purchased from the ATCC. MDA-MB-231, MCF7, and A549 cells were cultured in DMEM supplemented with 10% fetal bovine serum (FBS) (Invitrogen). HCC1806, T47D, and ZR-75-1 cells were cultured in RPMI supplemented with 10% FBS. All other cells were maintained in MEM supplemented with 10% FBS and 10 μg/ml insulin (Sigma-Aldrich). The authenticity of the cell lines was confirmed through STR profiling, and they undergo monthly testing for *mycoplasma* contamination. The following antibodies were used in this study: p-AKT-Ser473, AKT, EGFR, NRP1 (Cell Signaling), p-serine (Millipore), p-EGFR, NRP1 (Abcam), EGFR, calpain 2, actin, talin (Santa Cruz), HA (Sigma), GAPDH (Genetex), streptavidin-PE, and alkaline phosphatase-conjugated secondary antibodies (Jackson ImmunoResearch). The following proteins, lectins, or reagents were used in the study: biotinylated peanut agglutinin (PNA, Vector Labs), agarose-bound PNA (Vector Labs), recombinant hEGF (Sigma), recombinant hEGFR (R&D), and magnetic xMAP beads (MagPlex) (Luminex). The control (pLAS. Void/pVoid), *ST3GAL1* short hairpin RNA (shRNA) (TRCN0000231843), *NRP1* shRNA-1 (TRCN0000322980), and *NRP1* shRNA-2 (TRCN0000322983) plasmids were purchased from the RNAi core (Academia Sinica).

Quantitative real-time PCR (qRT−PCR) analysis

Total RNA was isolated using TRIzol reagent (Invitrogen), and cDNA was generated from 1000 ng of total RNA using a High-Capacity cDNA Reverse Transcription Kit (Applied BioSystems/ABI). qRT−PCR assays were performed using SYBR Green MasterMix (Applied Biosystems) on an ABI 7500 detection system (Applied Biosystems). The reference sequences for each primer are listed in Table S1. GAPDH was used as an internal control.

Transwell migration and invasion assays

For cell migration, the cells were serum-starved overnight. A total of 1 x 10^5 cells were resuspended in serum-free medium and plated into the upper chamber of the Transwell system, and the lower chamber was filled with complete culture medium or 100 ng/ml EGF in serum free media. The cells were allowed to migrate for 8 h. For the invasion assay, the inserts were coated with Matrigel at 37 °C overnight. Onex10^6 cells were resuspended in serum-free medium and plated into the upper chamber of a Transwell (Corning), and the lower chamber was filled with complete culture medium. The cells were allowed to migrate for 24 h. The cells on the inner surface of the inserts were gently removed, and the inserts were fixed and stained with 0.2% crystal violet in 10% EtOH for 10 min. After washing with PBS 3 times, the number of cells in five random fields was counted at 400 × magnification using a light microscope (Leica).

Time-lapse in vitro *scratch assay*

ST3GAL1-silenced or control cells were serum-starved overnight. The cells were wounded using sterile pipette tips (T = 0 h) and washed with PBS, and the medium was replaced with complete medium. Cell migration was monitored at 30-min intervals using a real-time system (IncuCyte).

Analysis of glycopeptide in-gel release by LC–MS/MS

NRP1 was excised *via* NuPAGE and digested with trypsin. The digested glycopeptides were purified using 1 cc of Sep-Pak tC18 (WAT054960). In brief, the columns were equilibrated using 1 ml 100% acetonitrile (ACN) and washed twice with 0.1% trifluoroacetic acid (TFA). The digested glycopeptides were added to 200 μl of 0.1% TFA and loaded into the columns. After washing with 1 ml of 0.1% TFA twice, the cells were washed with 200 μl of 0.5% acetic acid. The digested glycopeptides were eluted with 75% acetonitrile/0.5% acetic acid. The eluted peptides were dried and dissolved in 0.1% (v/v) formic acid for nanoLC-MS/MS using an Orbitrap Fusion mass spectrometer (Thermo Scientific) equipped with a nanoelectrospray ion source (New Objective) and an UltiMate 3000 RSLCnano system pump (Thermo Scientific Dionex). Nanoflow LC for the separation of *O*-glycans was conducted at a flow rate of 300 nl/min with a linear gradient from 25% (v/v) acetonitrile to 55% (with 0.1% formic acid) for 45 min. The nanoelectrospray source was powered in the range of 1.6 to 1.8 kV. The scan cycle was performed in top-speed mode within a cycle time of 3 s, which can intelligently schedule MS

and data-dependent MS/MS scans. The full-scan MS (m/z 300–2000) experiment was performed in the Orbitrap at a resolution of 120 K and an automatic gain control (AGC) target value of 4 × 1018, while the data-dependent MS/MS experiments were conducted in the C-trap using higher energy collisional dissociation (HCD) with 15% normalized collision energy at a resolution of 15 K and an AGC value of 5 × 108. PMI-Byonic has been used for MS/MS-based protein and glycosylation site identification (44). Protein identification was based on the canonical *Homo sapiens* UniProt database, which included 71,591 protein sequences. C-terminal cleavage of lysine and arginine and a maximum of two missed cleavages were allowed. Tolerances of 10 ppm and 20 ppm were applied to the precursor and fragment ions, respectively. Carbamidomethylation was set as a fixed modification of cysteine residues. Methionine oxidation was used as a variable modification. *N*-glycopeptides were searched against the database "*N*-glycan 309 mammalian no sodium." *O*-glycopeptides were searched against "78 mammalian" sequences. We next loaded the peak list into the analytic module of GlycoWorkbench to annotate the peak with the glycan structure from the CFG database according to the MS correlation with 5 ppm tolerance. We manually examined the MS/MS spectra of matched *O*-glycan structures and annotated carbohydrate fragmentation based on the nomenclature proposed by Domon and Costello (45).

PBMC-mediated cell lysis

Peripheral blood samples were collected from healthy volunteers following the acquisition of written informed consent. All samples were fully anonymized and utilized in accordance with a protocol approved by the Institutional Review Board of the Human Subjects Research Ethics Committee at Chang Gung Memorial Hospital (Approval Number: 202102123B0). This study was conducted in compliance with the principles of the Declaration of Helsinki.

In brief, 1 x 10^6 MDA-MB-231 cells/ml were incubated with BATDA (DELFIA EuTDA Cytotoxicity Reagents kit, PerkinElmer). BATDA-labeled cells (1 × 10^4) were transferred to a round-bottomed 96-well plate and mixed with a cancer-targeting antibody (control hIgG or cetuximab). PBMCs were isolated from the blood of healthy donors by density gradient centrifugation using Ficoll-Paque (Amersham Biosciences, Uppsala, Sweden), washed twice with PBS, resuspended at 1 × 10^5 cells/ml in the same culture medium used for the target cells, and incubated for an additional 120 min at 37 °C. To determine spontaneous release, BATDA-labeled cells were incubated in medium without effector cells. To evaluate the maximal release, complete cell lysis was induced by Triton X-100 (5% v/v final concentration). Following incubation, the plates were centrifuged (500×*g*, 5 min), and 20 µl of supernatant from each well was transferred to a flat-bottomed 96-well plate (Greiner). Finally, 100 µl of europium solution (Wallac) was added to each well, and the fluorescence of the EuTDA chelates was measured using a time-resolved fluorometer (VICTOR^3, PerkinElmer). The percentage of specific release was calculated as 100% (experimental release - spontaneous release)/(maximal release - spontaneous release). All tests were performed in triplicate. This study was approved by the Institutional Review Board of the Human Subjects Research Ethics Committee of the Chang Gung Memorial Hospital.

Plasmids and protein purification

The gene encoding full-length human NRP1 (NM_003873.7) was cloned and inserted into the CloneJET PCR cloning kit (Thermo Fisher Scientific). After sequencing, an HA tag (YPYDVPDYA) was introduced after the signal peptide of NRP1. The corresponding HA-NRP1 construct was then subcloned and inserted into the pSIN-EF2-puro expression plasmid. MDA-MB-231 cells transfected with control or *shST3GAL1* stable clones were transfected with the HA-NRP1 construct using Lipofectamine 2000, followed by puromycin selection. The expression of HA-tagged NRP1 in the culture media was confirmed by western blotting using an anti-HA antibody. HA-tagged proteins in the culture media were incubated with an anti-HA monoclonal antibody-conjugated agarose gel (Sigma–Aldrich). After washing away residual impurities, bound HA-NRP1 can be eluted from the affinity column by the HA peptide according to the manufacturer's manual (Sigma). Proteins were quantified using a Pierce BCA Protein Assay Kit (Thermo Fisher Scientific). The purified proteins were validated using MASS Spectrum analysis.

Luminex-based protein–protein interaction assays

The assay was performed according to the manufacturer's instructions (xMAP Cookbook, third edition). Briefly, recombinant hEGF coupled with magnetic beads (MagPlex) was incubated with hEGFR overnight at 4 °C. After washing three times with washing buffer (1% PBS-BSA), the beads were equally divided into 96-well plates for different reactions. For the binding assay, serial dilutions of biotinylated HA-NRP1 (in 1% PBS-BSA for 2 h) were used for interactions. For final detection, streptavidin-PE (1:50 in 1% PBS-BSA, 30 min) was added and incubated for 30 min. Finally, the plate was washed and analyzed using a Luminex 200 instrument. For the control assay, EGF-coupled beads were incubated with 1% without HA-NRP1. xPonent software was used for the assay protocol and certificate analysis.

Calpain zymography

Casein zymography was used to determine the proteolytic activity of calpain 1 (CAPN1) and calpain 2 (CAPN2). Casein zymography was performed as described by Veiseth *et al.* (2001) (46). Briefly, 20 µg of cell lysate was subjected to electrophoresis on 0.21% casein and 12.5% nondenaturing PAGE. Then, the gel was incubated in reactivation buffer supplemented with 50 mM Tris, 0.05% 2-mercaptoethanol, and 4 mM CaCl2 (pH 7.5). After staining with Coomassie Brilliant Blue and destaining with 20% methanol and 7% acetic acid, calpain activity was visualized as clear bands against a dark background. The gels were photographed and quantified using GelPro31 software.

FLOW cytometry

Cells were harvested using 2 mM EDTA/1% BSA/PBS, washed with PBS, and resuspended in serum free DMEM/1% BSA. Cells were stained with 0.5 ug/ml Cetuximab or NRP1 for 30 min at 4 °C. The cells were then washed with PBS and stained with AF488-conjugated goat anti-human IgG or goat anti-rabbit IgG for 30 min at 4 °C. The cells were washed with PBS and analyzed using *Accuri C6 Plus* (BD). The data were further processed using FlowJo software (v10.9.0).

Data source, processing, and statistical analysis

Gene expression profiles and clinical information were obtained from the Gene Expression Omnibus (GEO) database (GEO accession: GSE47561, https://www.ncbi.nlm.nih.gov/gds/?term=GSE47561), which contains microarray data from 1570 breast cancer-related samples. The data are presented as the mean ± standard deviation (SD). The nonparametric Wilcoxon two-sample test was used to assess differences in ST3GAL family gene expression between breast cancer patients (others were considered the baseline group). A p value indicating less significance was set at $p < 0.05$. The prognostic values of ST3GAL1 and NRP1 were evaluated using receiver operating characteristic (ROC) area under the curve (AUC) analysis, and the Youden index (sensitivity + specificity − 1) was calculated to determine the optimal cutoff values for high *versus* low gene expression levels. Survival curves were plotted using the Kaplan–Meier method, with the log-rank test applied for comparison. The Cox proportional hazards regression model was used to identify the independent prognostic factors. Statistical computations were performed using Prism 7.0 (GraphPad Software) and SPSS V22.0 (IBM) software.

Ethics approval and consent to participate

Peripheral blood was collected from healthy volunteers after written consent was obtained. The samples were fully encoded and used according to a protocol approved by the Institutional Review Board of Human Subjects Research Ethics Committee of the Chang Gung Memorial Hospital (approval number: 202102123B0).

Consent for publication

Blood donors provided informed consent for publication of all the data included in the manuscript.

Data availability

The data that support the findings of this study are available upon reasonable request from the corresponding author.

Supporting information—This article contains supporting information.

Acknowledgment—We are grateful to Dr Jin-Yuh Shew of Academia Sinica for providing the ZR-75-1 cell line.

Author contributions—T. F. writing–original draft; T. F. methodology; T. F., A. Y. conceptualization; T. F., J. Y., S. C., and A. Y. funding acquisition; H. Y. and N. C. investigation; H. Y. and N. C. resources; T. H. software; T. H. formal analysis; Y. T., J. Y., S. C., and A. Y. writing–review & editing; J. Y., S. C., and A. Y. supervision.

Funding and additional information—This work was supported by grants from the National Science and Technology Council in Taiwan, NSTC 112 to 2314 B-182A-047 (TF), Chang Gung Medical Foundation, CMRPG3K2221 (TF), CMRPG3M0951 (TF), CMRPG3K0311 (SC) and OMRPG3C0048 (AY).

Conflict of interests—The authors declare that they have no conflicts of interest with the contents of this article.

Abbreviations—The abbreviations used are: ADCC, Antibody-dependent cellular cytotoxicity; CAPN1, Calpain 1; CAPN2, Calpain 2; DMFS, Distant-metastasis-free survival; LC–MS/MS, Liquid chromatography-tandem mass spectrometry; NRP1, Neuropilin-1; PBMC, Peripheral blood mononuclear cells; PNA lectin, Peanut agglutinin lectin; RFS, Relapse-free survival; ST3GAL1, ST3 beta-galactoside alpha-2,3-sialyltransferase 1.

References

1. Vajaria, B. N., Patel, K. R., Begum, R., and Patel, P. S. (2016) Sialylation: an avenue to target cancer cells. *Pathol. Oncol. Res.* **22**, 443–447. https://doi.org/10.1007/s12253-015-0033-6
2. Semel, A. C., Seales, E. C., Singhal, A., Eklund, E. A., Colley, K. J., and Bellis, S. L. (2002) Hyposialylation of integrins stimulates the activity of myeloid fibronectin receptors. *J. Biol. Chem.* **277**, 32830–32836. https://doi.org/10.1074/jbc.M202493200
3. Seales, E. C., Shaikh, F. M., Woodard-Grice, A. V., Aggarwal, P., McBrayer, A. C., Hennessy, K. M., *et al.* (2005) A protein kinase C/Ras/ERK signaling pathway activates myeloid fibronectin receptors by altering beta1 integrin sialylation. *J. Biol. Chem.* **280**, 37610–37615. https://doi.org/10.1074/jbc.M508476200
4. Harduin-Lepers, A., Vallejo-Ruiz, V., Krzewinski-Recchi, M. A., Samyn-Petit, B., Julien, S., and Delannoy, P. (2001) The human sialyltransferase family. *Biochimie* **83**, 727–737
5. Burchell, J., Poulsom, R., Hanby, A., Whitehouse, C., Cooper, L., Clausen, H., *et al.* (1999) An alpha2,3 sialyltransferase (ST3Gal I) is elevated in primary breast carcinomas. *Glycobiology* **9**, 1307–1311
6. Fan, T. C., Yeo, H. L., Hsu, H. M., Yu, J. C., Ho, M. Y., Lin, W. D., *et al.* (2018) Reciprocal feedback regulation of ST3GAL1 and GFRA1 signaling in breast cancer cells. *Cancer Lett.* **434**, 184–195
7. Guo, H. F., and Vander Kooi, C. W. (2015) Neuropilin functions as an essential cell surface receptor. *J. Biol. Chem.* **290**, 29120–29126
8. Prud'homme, G. J., and Glinka, Y. (2012) Neuropilins are multifunctional coreceptors involved in tumor initiation, growth, metastasis and immunity. *Oncotarget* **3**, 921–939
9. Glinka, Y., Mohammed, N., Subramaniam, V., Jothy, S., and Prud'homme, G. J. (2012) Neuropilin-1 is expressed by breast cancer stem-like cells and is linked to NF-kappaB activation and tumor sphere formation. *Biochem. Biophys. Res. Commun.* **425**, 775–780
10. Luo, M., Hou, L., Li, J., Shao, S., Huang, S., Meng, D., *et al.* (2016) VEGF/NRP-1axis promotes progression of breast cancer via enhancement of epithelial-mesenchymal transition and activation of NF-kappaB and beta-catenin. *Cancer Lett.* **373**, 1–11
11. Ding, Y., Zhou, J., Wang, S., Li, Y., Mi, Y., Gao, S., *et al.* (2018) Anti-neuropilin-1 monoclonal antibody suppresses the migration and invasion of human gastric cancer cells via Akt dephosphorylation. *Exp. Ther. Med.* **16**, 537–546
12. Naik, A., Al-Zeheimi, N., Bakheit, C. S., Al Riyami, M., Al Jarrah, A., Al Moundhri, M. S., *et al.* (2017) Neuropilin-1 associated molecules in the

blood distinguish poor prognosis breast cancer: a cross-sectional. *Study Sci. Rep.* **7**, 3301
13. Suo, Z., and Nesland, J. M. (2002) Type 1 protein tyrosine kinases in breast carcinoma: a review. *Ultrastruct Pathol.* **26**, 125–135
14. Sebastian, S., Settleman, J., Reshkin, S. J., Azzariti, A., Bellizzi, A., and Paradiso, A. (2006) The complexity of targeting EGFR signalling in cancer: from expression to turnover. *Biochim. Biophys. Acta* **1766**, 120–139
15. Normanno, N., De Luca, A., Bianco, C., Strizzi, L., Mancino, M., Maiello, M. R., *et al.* (2006) Epidermal growth factor receptor (EGFR) signaling in cancer. *Gene* **366**, 2–16
16. Tsutsui, S., Ohno, S., Murakami, S., Hachitanda, Y., and Oda, S. (2002) Prognostic value of epidermal growth factor receptor (EGFR) and its relationship to the estrogen receptor status in 1029 patients with breast cancer. *Breast Cancer Res. Treat.* **71**, 67–75
17. Shetty, S. R., Yeeravalli, R., Bera, T., and Das, A. (2021) Recent advances on epidermal growth factor receptor as a molecular target for breast cancer therapeutics. *Anticancer Agents Med. Chem.* **21**, 1783–1792
18. Park, J. J., Yi, J. Y., Jin, Y. B., Lee, Y. J., Lee, J. S., Lee, Y. S., *et al.* (2012) Sialylation of epidermal growth factor receptor regulates receptor activity and chemosensitivity to gefitinib in colon cancer cells. *Biochem. Pharmacol.* **83**, 849–857
19. Wang, C., Yang, Y., Yang, Z., Liu, M., Li, Z., Sun, L., *et al.* (2009) EGF-mediated migration signaling activated by N-acetylglucosaminyltransferase-V via receptor protein tyrosine phosphatase kappa. *Arch. Biochem. Biophys.* **486**, 64–72
20. Ankenbauer, K. E., Rao, T. C., Mattheyses, A. L., and Bellis, S. L. (2023) Sialylation of EGFR by ST6GAL1 induces receptor activation and modulates trafficking dynamics. *J. Biol. Chem.* **299**, 105217
21. Liu, Y. C., Yen, H. Y., Chen, C. Y., Chen, C. H., Cheng, P. F., Juan, Y. H., *et al.* (2011) Sialylation and fucosylation of epidermal growth factor receptor suppress its dimerization and activation in lung cancer cells. *Proc. Natl. Acad. Sci. U.S.A* **108**, 11332–11337
22. Rizzolio, S., Rabinowicz, N., Rainero, E., Lanzetti, L., Serini, G., Norman, J., *et al.* (2012) Neuropilin-1-dependent regulation of EGF-receptor signaling. *Cancer Res.* **72**, 5801–5811
23. Zhang, P., Chen, L., Zhou, F., He, Z., Wang, G., and Luo, Y. (2023) NRP1 promotes prostate cancer progression via modulating EGFR-dependent AKT pathway activation. *Cell Death Dis.* **14**, 159
24. Pellet-Many, C., Frankel, P., Jia, H., and Zachary, I. (2008) Neuropilins: structure, function and role in disease. *Biochem. J.* **411**, 211–226
25. Windwarder, M., Yelland, T., Djordjevic, S., and Altmann, F. (2016) Detailed characterization of the O-linked glycosylation of the neuropilin-1 c/MAM-domain. *Glycoconj. J.* **33**, 387–397
26. Pereira, M. E., Kabat, E. A., Lotan, R., and Sharon, N. (1976) Immunochemical studies on the specificity of the peanut (Arachis hypogaea) agglutinin. *Carbohydr. Res.* **51**, 107–118
27. Yeo, H. L., Fan, T. C., Lin, R. J., Yu, J. C., Liao, G. S., Chen, E. S., *et al.* (2019) Sialylation of vasorin by ST3Gal1 facilitates TGF-beta1-mediated tumor angiogenesis and progression. *Int. J. Cancer* **144**, 1996–2007
28. Lin, W. D., Fan, T. C., Hung, J. T., Yeo, H. L., Wang, S. H., Kuo, C. W., *et al.* (2021) Sialylation of CD55 by ST3GAL1 facilitates immune evasion in cancer. *Cancer Immunol. Res.* **9**, 113–122
29. Pietrobono, S., Anichini, G., Sala, C., Manetti, F., Almada, L. L., Pepe, S., *et al.* (2020) ST3GAL1 is a target of the SOX2-GLI1 transcriptional complex and promotes melanoma metastasis through AXL. *Nat. Commun.* **11**, 5865
30. Wu, X., Zhao, J., Ruan, Y., Sun, L., Xu, C., and Jiang, H. (2018) Sialyltransferase ST3GAL1 promotes cell migration, invasion, and TGF-beta1-induced EMT and confers paclitaxel resistance in ovarian cancer. *Cell Death Dis.* **9**, 1102
31. Yin, L., Qi, X. W., Liu, X. Z., Yang, Z. Y., Cai, R. L., Cui, H. J., *et al.* (2020) Icaritin enhances the efficacy of cetuximab against triple-negative breast cancer cells. *Oncol. Lett.* **19**, 3950–3958
32. Rimawi, M. F., Shetty, P. B., Weiss, H. L., Schiff, R., Osborne, C. K., Chamness, G. C., *et al.* (2010) Epidermal growth factor receptor expression in breast cancer association with biologic phenotype and clinical outcomes. *Cancer* **116**, 1234–1242. https://doi.org/10.1002/cncr.24816
33. Steplewski, Z., Sun, L. K., Shearman, C. W., Ghrayeb, J., Daddona, P., and Koprowski, H. (1988) Biological activity of human-mouse IgG1, IgG2, IgG3, and IgG4 chimeric monoclonal antibodies with antitumor specificity. *Proc. Natl. Acad. Sci. U.S.A* **85**, 4852–4856
34. Rosenstock, P., and Kaufmann, T. (2021) Sialic acids and their influence on human NK cell function. *Cells* **10**, 263
35. Rodriguez, E., Boelaars, K., Brown, K., Eveline Li, R. J., Kruijssen, L., Bruijns, S. C. M., *et al.* (2021) Sialic acids in pancreatic cancer cells drive tumour-associated macrophage differentiation via the Siglec receptors Siglec-7 and Siglec-9. *Nat. Commun.* **12**, 1270
36. Tanei, T., Choi, D. S., Rodriguez, A. A., Liang, D. H., Dobrolecki, L., Ghosh, M., *et al.* (2016) Antitumor activity of Cetuximab in combination with Ixabepilone on triple negative breast cancer stem cells. *Breast Cancer Res.* **18**, 6
37. Ferrara, N. (1999) Molecular and biological properties of vascular endothelial growth factor. *J. Mol. Med.* **77**, 527–543
38. Seifi-Alan, M., Shams, R., Bandehpour, M., Mirfakhraie, R., and Ghafouri-Fard, S. (2018) Neuropilin-1 expression is associated with lymph node metastasis in breast cancer tissues. *Cancer Manag. Res.* **10**, 1969–1974
39. Rachner, T. D., Kasimir-Bauer, S., Goebel, A., Erdmann, K., Hoffmann, O., Rauner, M., *et al.* (2021) Soluble Neuropilin-1 is an independent marker of poor prognosis in early breast cancer. *J. Cancer Res. Clin. Oncol.* **147**, 2233–2238
40. Zhang, J., Zhang, X., Li, Z., Wang, Q., Shi, Y., Jiang, X., *et al.* (2021) The miR-124-3p/neuropilin-1 Axis contributes to the proliferation and metastasis of triple-negative breast cancer cells and Co-activates the TGF-beta pathway. *Front Oncol.* **11**, 654672
41. Frankel, P., Pellet-Many, C., Lehtolainen, P., D'Abaco, G. M., Tickner, M. L., Cheng, L., *et al.* (2008) Chondroitin sulphate-modified neuropilin 1 is expressed in human tumour cells and modulates 3D invasion in the U87MG human glioblastoma cell line through a p130Cas-mediated pathway. *EMBO Rep.* **9**, 983–989
42. Arteaga, C. L., O'Neill, A., Moulder, S. L., Pins, M., Sparano, J. A., Sledge, G. W., *et al.* (2008) A phase I-II study of combined blockade of the ErbB receptor network with trastuzumab and gefitinib in patients with HER2 (ErbB2)-overexpressing metastatic breast cancer. *Clin. Cancer Res.* **14**, 6277–6283
43. Lin, H. H., Lee, H. W., Lin, R. J., Huang, C. W., Liao, Y. C., Chen, Y. T., *et al.* (2015) Tracking and finding slow-proliferating/quiescent cancer stem cells with fluorescent nanodiamonds. *Small* **11**, 4394–4402
44. Bern, M., Kil, Y. J., and Becker, C. (2012) Byonic: advanced peptide and protein identification software. *Curr. Protoc. Bioinformatics* **13**, 13.20.1–13.20.14
45. Domon, B., and Costello, C. E. (1988) A systematic nomenclature for carbohydrate fragmentations in FAB-MS/MS spectra of glycoconjugates. *Glycoconjugate J.* **5**, 397–409
46. Veiseth, E., Shackelford, S. D., Wheeler, T. L., and Koohmaraie, M. (2001) Effect of postmortem storage on mu-calpain and m-calpain in ovine skeletal muscle. *J. Anim. Sci.* **79**, 1502–1508